LAWRENCE
LIVERMORE
NATIONAL
LABORATORY

UCRL-PROC-208886

Intracavity, adaptive correction of a high-average-power, solid-state, heat-capacity laser

K. N. LaFortune, R. L. Hurd, J. M. Brase, R. M. Yamamoto

January 7, 2005

Society of Photo-Optical Instrumentation Engineers Photonics West
San Jose, CA, United States
January 22, 2005 through January 27, 2005

Intracavity, adaptive correction of a high-average-power, solid-state, heat-capacity laser

K. N. LaFortune, R. L. Hurd, J. M. Brase, R. M. Yamamoto

Lawrence Livermore National Laboratory

ABSTRACT

The Solid-State, Heat-Capacity Laser (SSHCL) program at Lawrence Livermore National Laboratory is a multi-generation laser development effort scalable to the megawatt power levels. Wavefront quality is a driving metric of its performance. A deformable mirror with over 100 degrees of freedom situated within the cavity is used to correct both the static and dynamic aberrations sensed with a Shack-Hartmann wavefront sensor. The laser geometry is an unstable, confocal resonator with a clear aperture of 10 cm x 10 cm. It operates in a pulsed mode at a high repetition rate (up to 200 Hz) with a correction being applied before each pulse. Wavefront information is gathered in real-time from a low-power pick-off of the high-power beam. It is combined with historical trends of aberration growth to calculate a correction that is both feedback and feed-forward driven. The overall system design, measurement techniques and correction algorithms are discussed. Experimental results are presented.

1. INTRODUCTION

The wavefront quality of laser is often a driving factor in its design, especially if the output is meant to propagate over large distances, be focused tightly onto a target or both. If care is not taken to control the spatial coherence or phase distribution across the output aperture, lasers can have poorer propagation characteristics than an incoherent source. The maximum performance achievable from a laser is a function of two things: 1) the (static) imperfections in the optical components used to construct it and 2) the (dynamic) aberrations induced during operation such as thermally-induced distortions. Lasers can be built with expensive components with tight tolerances, and they can be designed to minimize the impact of the thermal aberrations.[1] But, in the design of high-energy lasers, it is not always possible to design out all of the static or dynamic aberrations. In such cases, additional measures must be taken. One approach is the use of an adaptive optics control system similar to those used in astronomy.[2] Wavefront control of lasers using adaptive optics is nothing new. Typically, though, extra-cavity correction is employed because implementation is much easier than intracavity correction. However, intracavity correction provides additional benefits such as control over mode growth and output power. Implementing an adaptive optics control system inside a resonator is simple from an optomechanical point of view. But, it is difficult from an control standpoint because there is not a one-to-one correspondence between the phase that can be measured and the phase that needs to be applied as a correction. The relationship between an intracavity corrector and the phase sensor has been well developed for an unstable resonator.[3] It can be approximated by a geometrical model. Previous experimental attempts at intracavity correction of a laser's output with adaptive optics resulted in limited success.[4–6] The authors have demonstrated recent success in intracavity correction on a flashlamp-pumped, solid-state, heat-capacity laser.[7] Below, initial results on a similar, but more advanced, diode-pumped system are presented.

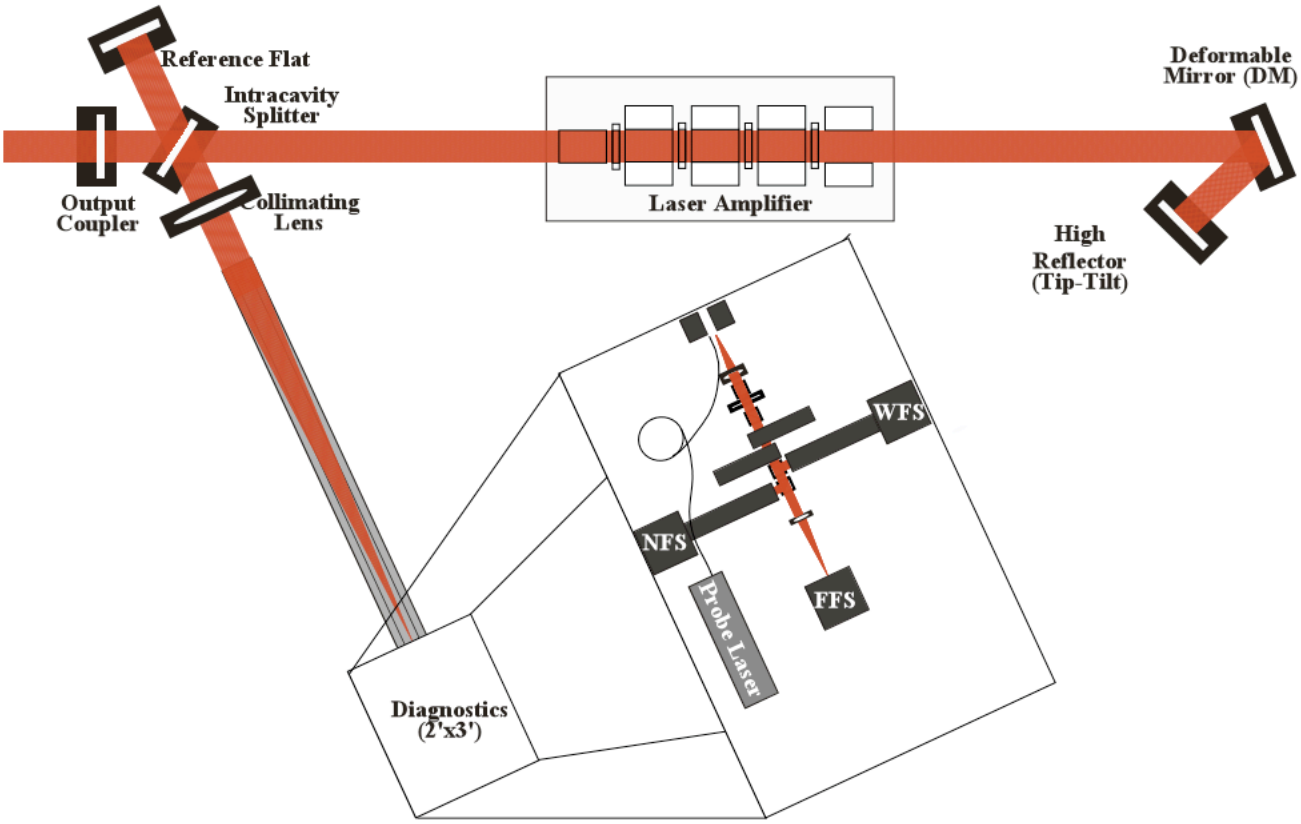

Figure 1. The system layout of the adaptively-corrected, unstable resonator on the diode-pumped, solid-state, heat-capacity laser test bed. Shown are the location of the gain media, resonator optics and diagnostic box. The amplifier contains four diode-pumped Nd:GGG slabs oriented normal to the optical axis of the cavity. The diodes pump the face of the slabs from a skew angle. The deformable mirror and tip-tilt correction are both at one end of the cavity. The output of the laser at the other end is a square annulus. The diagnostics measure the fully-filled 10 cm x 10 cm beam picked off just before the output. The laser's performance is measured in the near-field intensity, the far-field intensity and the gradient of its phase.

2. SYSTEM DESIGN

The intracavity, adaptive resonator (Figure 1), is incorporated into the third-generation, solid-state, heat-capacity laser (SSHCL) at LLNL.[8] It is a diode-pumped laser with over 10% electrical-to-optical efficiency. This laser is capable of producing over 30 kW of average power at 1062 nm. It is a pulsed laser, generating 500 μsec pulses at up to 200 Hz. It has been designed to run for bursts of up to 2000 shots before having to go through an active or passive cooling cycle. The clear aperture is a square 10 cm on a side. The geometry is a positive-branch, confocal, unstable resonator with a magnification of 1.5. The output profile of a laser with such a geometry is a square annulus with inner dimensions of 6 2/3 cm on a side.

There are some key differences between the specifications of this system and the flashlamp-pumped system on which adaptive control has already been demonstrated.[7] The obvious one is the pumping mechanism which has changed from flashlamps to diodes, bringing along with it an associated 10 fold boost in the overall system efficiency. The host material in the gain medium is different. This results in a slightly different operating

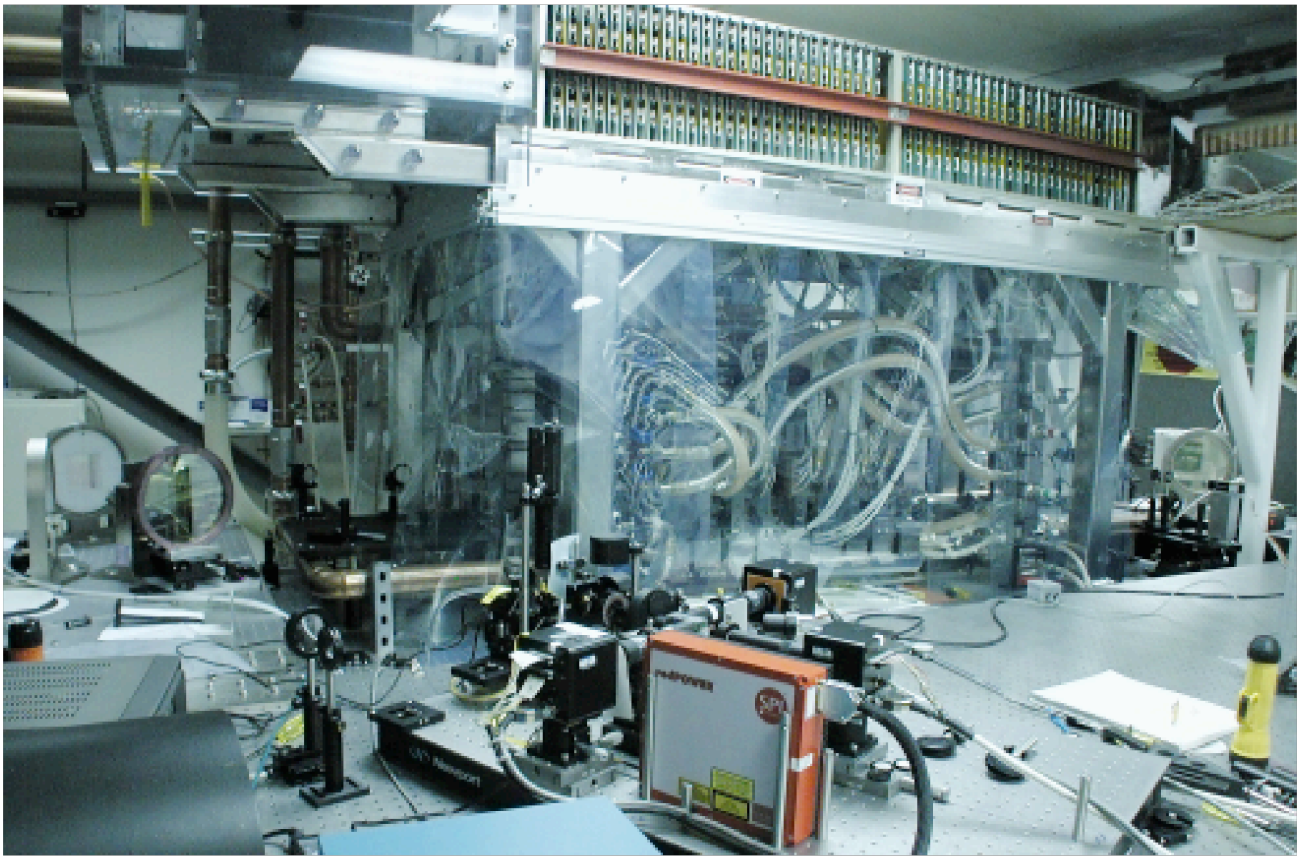

Figure 2. A photograph of the experimental setup. In the foreground is the diagnostic breadboard. Visible are the three diagnostic cameras and the fiber probe laser head. The laser output is to the left. To the far right, in the back, the deformable mirror is visible through the high-reflector end mirror of the laser cavity. In the center of the field are the laser slabs and associated diode arrays, cooling water and pulse-forming-network cards.

wavelength (1062 nm instead of 1053). The slabs are oriented normal to the optical axis versus being Brewster's angle. The net result is an unpolarized laser instead of a polarized one. The overall output has increased by more than three times through a combination of an increase in the rep rate of a factor of 10 and a drop in the pulse energy by a factor of three.

The adaptive-optics control system had to be adapted to accommodate these differences. Increasing the loop rate of the control system was simply a matter of buying a newer, faster computer than the dual 300 MHz CPU system that controlled the second-generation system. A redesign of the electronics hardware provided the opportunity to make several other upgrades such as full frame rate cameras in all diagnostics. The optical system had to be designed to take into account polarization effects not seen in the previous system. The necessity of a redesign of the optical system provided the opportunity to simplify and make more compact and hence more robust the diagnostics package. All three diagnostics and the reference source were combined into a single leg with a minimum propagation distance. The reference source was upgraded from a small diode-pumped laser with questionable spatial coherence to a 4 Watt, single-mode fiber laser manufactured by SPI, Inc. Switching

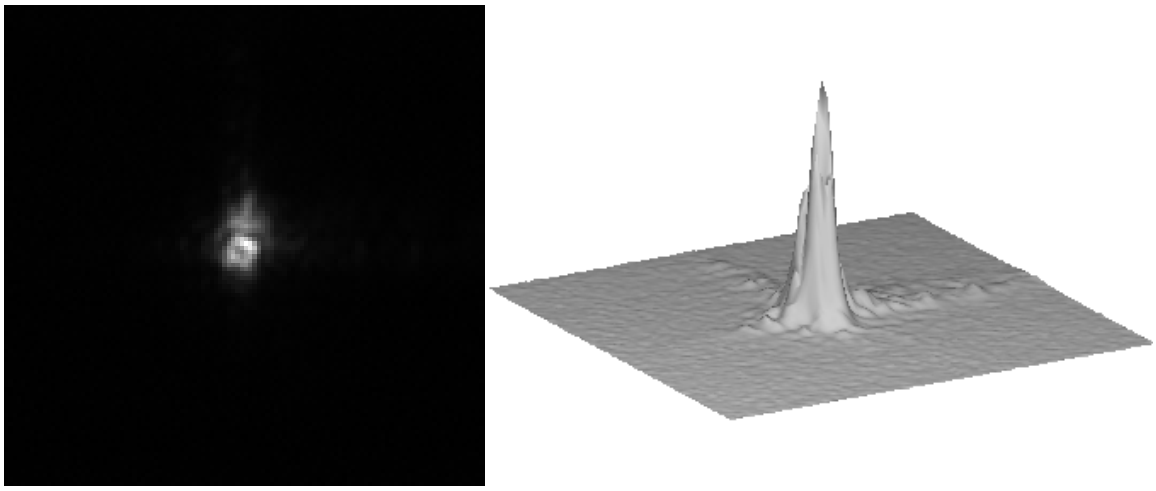

Figure 3. Linear 2D and 3D representations of a single pulse from a 100 pulse sequence.

to a fiber laser also provided the opportunity to make the system dichroic. A lasing wavelength close to that of the high-power beam of Ytterbium at 1090 nm was used. This wavelength is similar enough to the high-power lasing wavelength that dispersion effects are negligible but different enough that dichroic optics could be used to optimize output coupling of the high-power laser simultaneously to the diagnostic coupling of the probe laser.

The diagnostic sensors, DM hardware and their calibration method were essentially unchanged from the previous system except for some increase in sensitivity. The wavefront must be measured and controlled across the whole 10 cm by 10 cm area. Therefore, a beam-splitter is used within the cavity to couple out the full beam profile to the diagnostics. In addition to far-field and near-field diagnostics, there is a Shack-Hartmann wavefront sensor (WFS), which is used to measure the gradient of the phase. The WFS is composed of a rectangular array of 19 x19 lenslets mounted in front of a camera. The average phase within each sampling interval is measured. The sensor was designed for a sensitivity of $< \lambda/50$.

The deformable mirror (DM), located within the resonator cavity, is designed to work with the WFS to compensate for the measured aberrations. Manufactured by Xinetics Corp., it has a ULE face-sheet, supported by 206 PMN actuators on a pseudo-hexagonal grid with a nominal 1 cm actuator spacing and a dynamic range of 10 μm. There are 126 actuators within the clear aperture of the laser. The surface was polished to a tolerance of $< \lambda/50$ RMS powered figure and coated with a high-damage-threshold, high-reflectivity, multilayer-dielectric coating.

The WFS is calibrated with the fiber probe laser. First, the probe beam is sent directly to the WFS, bypassing the cavity, to measure a reference point. Then the probe laser is propagated one round trip through the cavity. Each actuator on the DM that is within the clear aperture is pushed, one at a time. The WFS response to each actuator push is recorded as the system impulse response. From the impulse response measurements of all the actuators, a matrix can be built that applies a least-squares fit of the DM surface to any measured wavefront

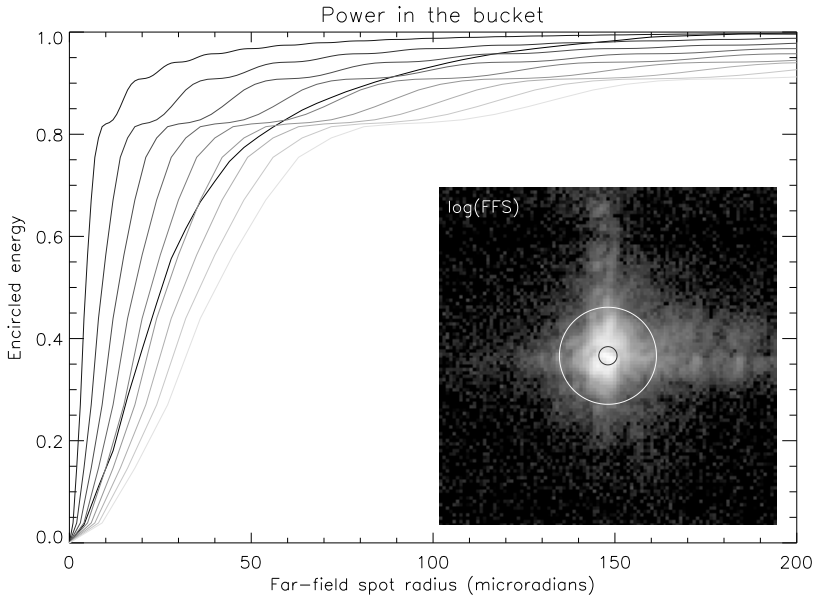

Figure 4. Power-in-a-bucket curve of a single pulse from a 100 pulse sequence. The darkest curve is the measured power-in-the-bucket, or encircled-energy, curve of a single pulse. The lighter curves depict the encircled energy within the theoretical, or diffraction-limited, pulse and integer multiples thereof. Referencing to these contours, for any desired cut-off, a "times-diffraction-limited", or xDL number can be determined. The diffraction limited spot size is the radius to the first minimum of the far-field pattern. The inset is a logarithmic plot of the measured far-field diffraction pattern. The superimposed circles encompass the diffraction limited area for the theoretical curve (smaller circle), and the measured curve (larger circle). The correctable spatial frequency domain of the and the spatial frequency domain of the DM (largest). The horizontal scale is the divergence angle assuming 1 μm light propagating from a 10 cm aperture.

error.

Before operation, most of the static aberrations can be removed by closing the control loop on the probe laser. This gives the laser a good starting point for laser operation. The really good performance does not occur until the WFS measures the active beam. It receives a low-power pick-off of the high power beam. The control system then applies a correction based on the error it sees plus an anticipated shot-to-shot induced error. The combination of the feedback and feed-forward signals each contribute to the overall correction.

3. EXPERIMENTAL RESULTS

The commissioning of the laser took place over the past year. The system specifications and design were established at the beginning of 2004 once all of the engineering details learned on the flashlamp-pumped system had been incorporated and verified. The components were ordered early in the year while experiments were still being performed on the older generation system. The transition from the experimental effort on the older system to the construction effort on the newer system occurred once most of the components were in-hand in September. Assembly, alignment and system integration proceeded through October and November. The laser aberrations were precorrected with the probe laser. First results from loop closure on the high-power beam were achieved in December. Data from these first experiments appear in the figures.

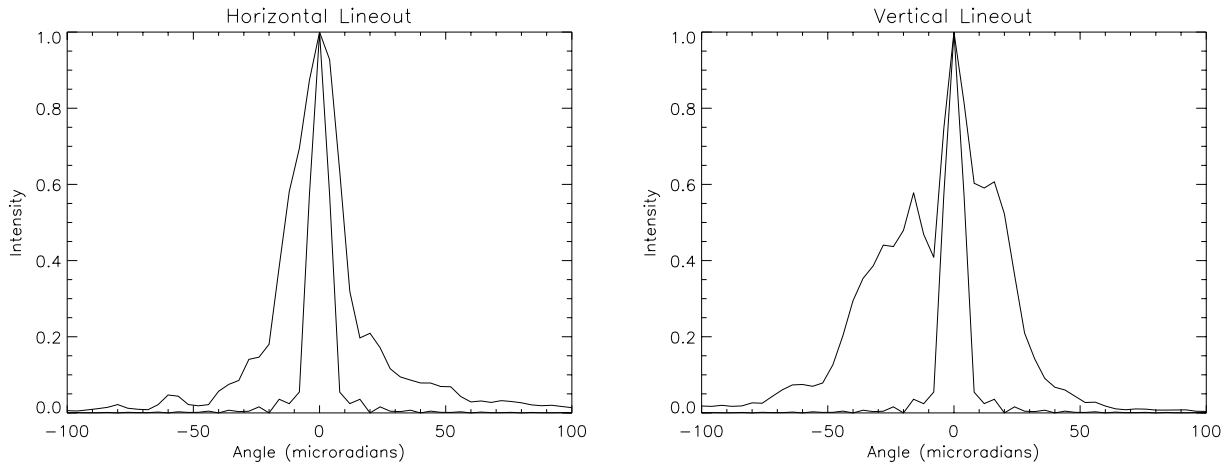

Figure 5. Horizontal and vertical line-outs of a single pulse from a 100 pulse sequence. Two traces appear in each graph. The thin line is the theoretical curve, sampled at the resolution of the far-field imaging array. The thick line is the peak-normalized measured intensity curve obtained from the far-field imaging array. The horizontal scale is measured in terms of the far-field angular divergence of a spatially coherent 10 cm x 10 cm beam of $\lambda = 1.06\mu$m light.

There are many metrics, and conventions within each metric, by which a laser's wavefront quality can be measured. The ratio of the actual spot radius to the theoretical limit, or "times-diffraction-limit" (xDL) number is a generally useful metric but is somewhat arbitrary. Different conventions are used to determine the nominal radius. It may correspond to the radius at which the first minimum in far-field distribution occurs. It may correspond to the full-width, half-maximum (FWHM) or the 1/e point among others. Although the temptation to reduce the wavefront quality to one number is great, a more descriptive metric is the encircled-energy, or power-in-a-bucket (PIB), curve. It is a plot of the fraction of energy contained within a xDL radius as a function of the radius. It essentially shows the xDL number for any arbitrary convention. It is, by definition, zero at a radius of zero and one at a radius of infinity. In between, one can find the xDL size (using any desired convention). The fraction of energy deposited within any desired divergence angle can be obtained. For well confined energy distributions, a Strehl ratio can also be estimated from the figure as the fraction of the energy within a 1xDL radius. A power-in-a-bucket curve for one of the pulses in a 100 shot run presented above appears in Figure 4. Overlaid on the curve are several, scaled curves of the theoretical encircled energy distribution. They correspond to spots that are 1, 2 , 3 etc. times the diffraction limit. The xDL number for the measured curve at any energy fraction can be determined by establishing which curves the measured curve lies between. Linear two-dimensional and three-dimensional representations of the pulse shape appear if Figure 3. Line-outs of the same pulse appear in Figure 5. To perform a reliable PIB measurement, a 12 bit camera with low read noise (< 2 counts) and a large area needed to be used. Careless background subtraction or lower bit-depth can result in artificially low xDL values.

4. CONCLUSION

Adaptive correction of a high-power, diode-pumped, solid-state, heat-capacity laser with an intracavity deformable mirror has been demonstrated. The control signal was derived from the actual, high-power beam. The control loop repetition rate is 200 Hz, an order of magnitude faster than previously demonstrated correction. Power-in-a-bucket measurements put the initial performance of the beam at about the same performance level as was achievable on the old system only after much fine-tuning. This system has improved stability and sensitivity over the older, flashlamp-pumped system. Performance will now be optimized.

Acknowledgements

Supported by U.S. Army Space and Missile Defense Command. This work was performed under the auspices of the U.S. Department of Energy by University of California, Lawrence Livermore National Laboratory under Contract W-7405-Eng-48. UCRL number: UCRL-PROC-208886

REFERENCES

1. J. Vetrovec, "Solid-state high-energy laser," *Proc. SPIE* **4632**, pp. 104–14, 2002.
2. C. E. Max, D. T. Gavel, and S. S. Olivier, "Near infra-red astronomy with adaptive optics and laser guide stars at the keck observatory," *Proc. SPIE* **2534**, pp. 412–22, 1995.
3. K. E. Oughstun, "Aberration sensitivity of unstable-cavity geometries," *J. Opt. Soc. Am. A - Optics & Image Science* **3**, pp. 1113–41, Aug. 1986.
4. J. M. Spinhirne, D. Analfi, R. H. Freeman, and H. R. Garcia, "Intracavity adaptive optics. i. astigmatism correction performance," *App. Opt.* **20**, p. 976, 1981.
5. D. Analfi, J. M. Spinhirne, R. H. Freeman, H. R. Garcia, and K. E. Oughstun, "Intracavity adaptive optics. ii. tilt correction performance," *App. Opt.* **20**, p. 1926, 1981.
6. K. E. Oughstun, J. M. Spinhirne, and D. Anafi, "Intracavity adaptive optics. iv. comparison of theory and experiment," *Appl. Opt.* **23**, pp. 1529–41, May 1984.
7. K. N. LaFortune, R. L. Hurd, E. M. Johansson, B. D. Dane, S. N. Fochs, and J. M. Brase, "Intracavity adaptive correction of a 10-kw solid state heat-capacity laser," *Proc. SPIE-Int. Soc. Opt. Eng.* **5333**, pp. 53–61, June 2004.
8. M. D. Rotter, C. B. Dane, S. Fochs, K. LaFortune, R. Merrill, and B. Yamamoto, "Solid-state heat-capacity lasers: Good candidates for the marketplace," *Photonics Spectra* **38**(8), 2004.